Received: 20 April 2017 | Revised: 25 September 2017 | Accepted: 13 December 2017

DOI: 10.1002/eco.1936

RESEARCH ARTICLE

WILEY

Forest composition effect on wildfire pattern and run-off regime in a Mediterranean watershed

Noa Ohana-Levi[1] | Amir Givati[2] | Tarin Paz-Kagan[1] | Arnon Karnieli[1]

[1] The Remote Sensing Laboratory, Jacob Blaustein Institutes for Desert Research, Ben-Gurion University of the Negev, Sede Boker Campus, Beersheba 84990, Israel

[2] Israeli Hydrological Service, Israel Water Authority, Jerusalem 91360, Israel

Correspondence
Arnon Karnieli, The Remote Sensing Laboratory, Jacob Blaustein Institutes for Desert Research, Ben-Gurion University of the Negev, Sede Boker Campus, Beersheba 84990, Israel.
Email: karnieli@bgu.ac.il

Funding information
European Union's Horizon 2020 Research and Innovation Programme, Grant/Award Numbers: 654359 and 641762; Ministry of Science and Technology via the Ramon Foundation, Israel, Grant/Award Number: 3-10673; Israel Water Authority, Grant/Award Number: 4500686906

Abstract

Fire may alter land cover throughout the landscape and affect run-off responses to rainfall events in a burnt watershed. Therefore, the challenge is to understand the interactions between forest composition and fire patterns in a karstic, Mediterranean watershed that affects the run-off regime. The aim of this research is to improve the understanding of the interactive effects of wildfire and land-cover change on the rainfall–run-off relationship in a first-order watershed. To achieve this goal, satellite imagery, official spatial data, and hydrological modelling were used to study forest composition in relation to extreme fire and to simulate run-off response for 2 rainfall events. The results show that an extreme wildfire had a greater impact on planted forest, composed mostly of pines, than on native species. Additionally, it was found that the land-cover alternation due to fire affected the run-off regime and contributed to an increase in maximum discharge and run-off volume for the 2 rainfall events by ~39–47%. During the regeneration period, the run-off response for the 2 rainfall events decreased by ~7.7–9%. Wildfires may impact the run-off response more profoundly as the plantation of pine trees increases. A greater increase in run-off response may endanger infrastructure in terms of flooding and affect the population well-being. Watershed management in areas where afforestation is considered should focus on planting native species that are less flammable rather than introducing combustible pines, thus reducing the hydrologic impacts of land-cover alteration due to wildfire, especially when climate warms and wildfires become more frequent and intense.

KEYWORDS

forest fire, hydrological model, land-cover change, remote sensing

1 | BACKGROUND

The number of forest fires in Mediterranean countries is constantly growing as human activity increases and the climate changes (Jolly et al., 2015; Wittenberg & Malkinson, 2009). These fires may change watershed characteristics, for example, reducing vegetation cover and increasing suspended sediment concentrations (Lane, Sheridan, & Noske, 2006), resulting in altered hydrologic responses to a specific precipitation regime (Moody & Martin, 2001). Land-cover (LC) alteration in a watershed, as a result of fire, may also lead to changes in run-off regime and amplify hydrological processes (Johansen, Hakonson, & Breshears, 2001). In this regard, several mechanisms were documented (Cydzik & Hogue, 2009; Moody & Martin, 2001; Soulis, Dercas, & Valiantzas, 2012; Tessler, Wittenberg, Malkinson, & Greenbaum, 2008; Wittenberg & Inbar, 2009; Woodsmith, Vache, McDonnell, & Helvey, 2004), including (a) a decrease in canopy interception that increases the portion of rainfall available for run-off; (b) a decrease in the loss of water to evapotranspiration, causing an increase in water availability for run-off; and (c) an alteration of the chemical and physical properties of the soil that are linked to water repellency. The impacts of wildfire on the hydrological regime, due to vegetation removal and regeneration of vegetation in Mediterranean areas, may last 5 to 10 years after the fire (Bosch & Hewlett, 1982; Wine & Cadol, 2016). The ecological recovery may also last several years/decades (Haim & Izhaki, 1994; Ne'eman, Lahav, & Izhaki, 1995). In addition to fire leading to reduction in the vegetative landscape, other land-cover changes (LCCs) can alter the hydrological response within a watershed (Costa, Botta, & Cardille, 2003), such as urbanization, afforestation, vegetation removal, and agricultural activities.

Representing spatial trends within burnt watersheds using remotely sensed and geographic information system techniques has been achieved in various ways, including expressing the spatial

frequency, density, and intensity of fires (Tessler, 2012; Tessler et al., 2011); focusing on fire scars and burnt versus unburnt areas (Fox et al., 2016; Levin & Heimowitz, 2012); and using vegetation indices (Leeuwen et al., 2010). However, the literature still lacks information on postfire LCC interactions, including forest composition and species distribution. Quantifications of the effects of fire-induced LCC on rainfall–run-off relations have been widely performed. Many studies used local approaches, such as plots along slopes within the study sites, to determine the effects of fire on run-off (Lane et al., 2006; Wittenberg & Inbar, 2009). Studies that considered the spatial patterns of the watershed through classification of the landscape often used statistically based approaches to quantify the relations between spatial changes due to fire and the affected run-off (Soulis et al., 2012; Wine & Cadol, 2016). Several studies used hydrological modelling techniques but did not consider species composition and their distribution throughout the landscape (Cydzik & Hogue, 2009). Despite these efforts, very few studies used spatial representation and pattern analysis of the entire watershed, along with hydrological simulations, in order to evaluate the run-off response prefire, postfire, and during the forest regeneration stages (Hallema et al., 2016; Rulli & Rosso, 2007). The current paper introduces an approach that includes both a representation of the spatial pattern of forest composition and the effect of the areal cover as a result of fire, as well as hydrological modelling of the run-off regime for three stages of the watershed: prefire, postfire, and during regeneration.

Different hydrological models are used for quantifying the hydrological effects of LCCs as a result of fire, such as Soil and Water Assessment Tool (Goodrich et al., 2005), Regional Hydro-Ecologic Simulation System (Tague, Seaby, & Hope, 2009), and Hydrologic Engineering Center's Hydrologic Modeling System (Papathanasiou, Alonistioti, Kasella, Makropoulos, & Mimikou, 2012). All of them benefit from the ability to input a wide range of parameters in order to simulate hydrographs for a given surface. Similarly, the Weather Research and Forecasting Hydro (WRF-Hydro) model is a high-resolution, event-based hydrological forecasting model that relies on forecasted or measured rainfall data as input to simulate the hydrological response to the predicted weather. It was developed to facilitate the representation of terrestrial hydrological processes related to the spatial redistribution of surface, subsurface, and channel waters and to carry out the coupling of hydrological models to atmospheric models. It has never been used for simulating postfire effects on the run-off regime. In the current study, a local, uncoupled version of the WRF-Hydro model (Givati, Gochis, Rummler, & Kunstmann, 2016) was used to study the effect of LCC and forest fire on run-off response following a large rainfall event.

Mount Carmel, Israel, has experienced an increasing number of wildfire events over the last three decades, resulting in hundreds of small fire events and 10 fires that consumed areas of more than 100 ha, caused mainly by anthropogenic factors (Tessler et al., 2011). An exceptional fire occurred on Mount Carmel, Israel, from December 2–6, 2010, covering an area of about 2,530 ha of natural forest and shrubs, as well as planted pine forest. Its ignition was at the outskirts of Carmel City along the higher elevations, caused by human activity, and strong eastern winds extended the fire quickly (within an hour) westwards, towards the forested slopes (Paz, Carmel, Jahashan, & Shoshany, 2011). This fire was one of the largest fire events ever recorded in Israel, causing the loss of 44 lives, along with infrastructure, and affecting ecological, biological, and hydrological processes (Tessler, 2012). The current study focused on this wildfire's effects on the run-off response in the Oren Watershed, located within the Carmel Forest. Approximately 38% of the forested landscape in this watershed was burned during the fire (Tessler et al., 2011), constituting about 12% of the total watershed area. High run-off discharge following fire events of this magnitude might affect the population activities in the watershed, for example, agriculture, main roads, and the quality of life of the few settlements throughout the watershed.

The hypotheses of the study were that with respect to the spreading path of the fire, different forest compositions and species distribution patterns within the forest would respond differently to fire, having an effect on the burning pattern and LCC within the watershed. Consequently, the decrease in tree cover would lead to an increase in run-off response that would gradually return to the normal regime after several years of the regeneration process. The aim was to improve the understanding of the interactive effects of wildfire and LCC on the rainfall–run-off relationship in a first-order watershed. The specific objectives were (a) to assess changes in land cover throughout the watershed by processing space-borne images from three key periods: before the wildfire occurred, shortly after the fire, and after 2 years of the recovery process; (b) to analyse the patterns and characteristics of the burnt area and assess their sensitivity to fire; and (c) to simulate run-off volume and discharge for different LC statuses (prefire, postfire, and during the recovery process).

2 | METHODS

2.1 | Study area

Mount Carmel is located in northern Israel (Figure 1a) and was declared by UNESCO as a biosphere reserve in 1996 (Frankenberg & Cohen, 1996). The Carmel Forest covers an area of about 250 km^2, reaching an elevation of 546 m above mean sea level (Inbar, Tamir, & Wittenberg, 1998). The lithology of the area is composed of carbonate marine sedimentary rocks. The pedology includes terra rossa soils on top of the hard limestone and dolomite rocks, whereas rendzina soils cover the soft marl and chalk rocks (Tessler et al., 2008). The Carmel area has a Mediterranean climate, with a long, dry summer season and a rainy winter season between November and April. The mean annual rainfall ranges between 550 mm along the coastal plain and 750 mm in the higher elevations (Inbar et al., 1998). The Oren Watershed is located in the Carmel Forest (Figure 1a), and its area is about 58 km^2 (Figure 1b). A hydrometric station is located within the stream and gauges a drainage area of about 25 km^2 (Figure 1b). The dominant flow regime in the Oren Watershed is flash floods, occurring during heavy rainfall events. It has a steep topography and is drained by an ephemeral mountain stream into the Mediterranean Sea. Mount Carmel is a karstic environment, with substantial vertical losses during rainfall events (Wittenberg, Kutiel, Greenbaum, & Inbar, 2007), depriving the stream network from consistent baseflow. The basin response time, as well as total flow time, is short, and the specific peak discharges are relatively low for a small Mediterranean watershed. This is attributed to the landscape that is mostly composed of dense

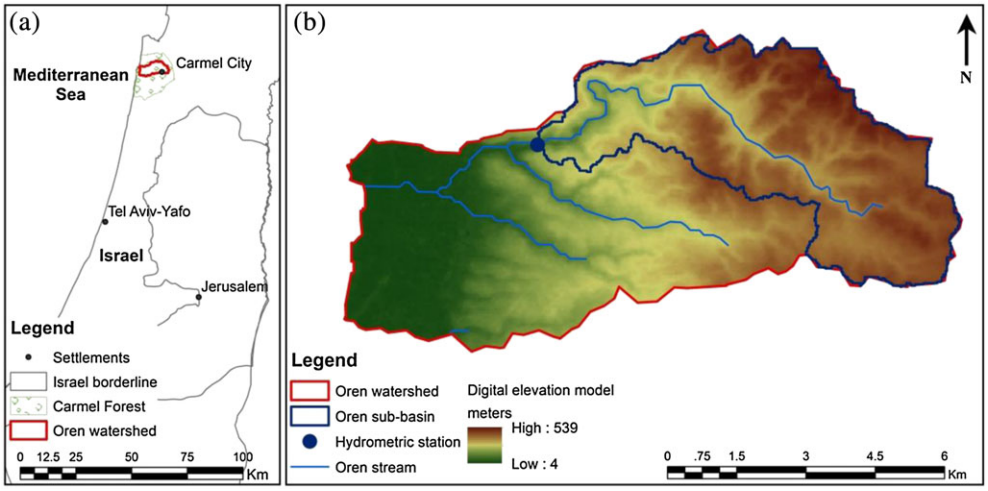

FIGURE 1 (a) The Oren Watershed study area within the domain of Israel and the Carmel Forest; (b) topography of the drainage area and the location of the hydrometric station

forests. Carmel City is located along the watershed's headwaters and is undergoing gradual urban expansion, including a building trend within the city's borders, as well as urban sprawl along its margins, at the expense of the bordering forest (Wittenberg & Malkinson, 2009).

Mount Carmel is covered by natural forest, composed mostly of oaks (*Quercus calliprinos*), terebinth (*Pistacia palaestina*), and planted forest, characterized by non-native species, predominantly pines (*Pinus halepensis*). The first plantings of pines occurred in the 19th century by German Templers. Later, during the British mandatory government from 1925 to 1929, more extensive afforestation was conducted, and later, more pines were introduced to this area by the Jewish National Fund between 1952 and 1966 (Wittenberg & Malkinson, 2009). During this period, the major objectives of afforestation in Israel were to protect public land, provide employment, and improve the landscape. Thus, the management approach focused on planting few species that required minimal care, with high establishment and growth rates, and that were adaptable to a large array of edaphic and climatic conditions. The *P. halepensis* was suitable for these motives and ensured rapid, low-cost afforestation over large areas in a short time (Osem, Ginsberg, Tauber, Atzmon, & Perevolotsky, 2008).

2.2 | The study framework

In order to study the effects of LCC due to fire, two rainfall events were chosen and used in hydrological model simulations with different LC maps. This way, it was possible to compare the reactions of specific run-off events to different LC scenarios. The LC raster maps were based on classified satellite images. The methodological steps (Figure 2) included the generation of three LC maps through a process of classifying satellite images. In addition, an analysis of the burnt area

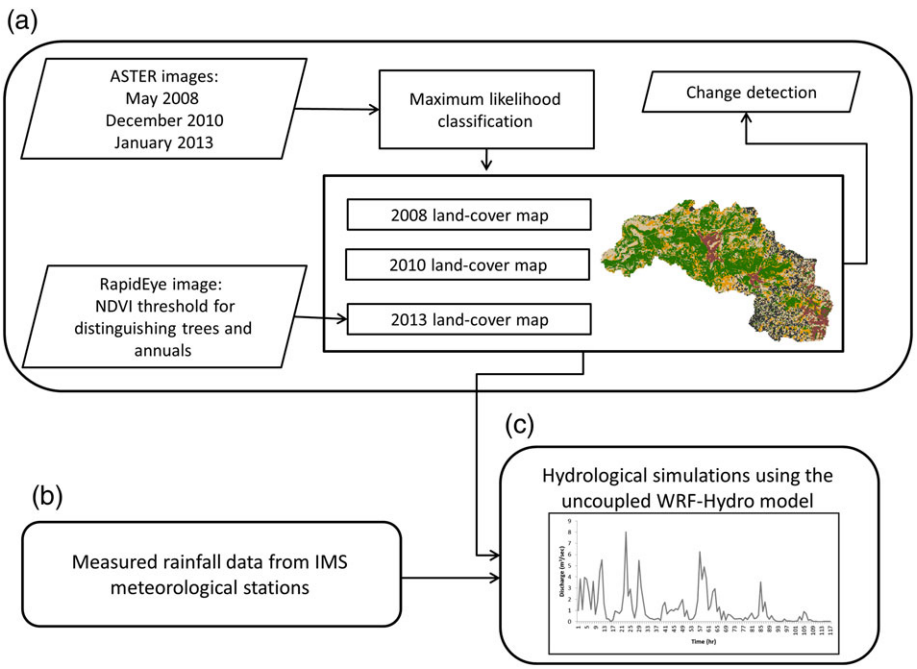

FIGURE 2 Outline of the study including three main stages: (a) the process of creating the three land-cover map; (b) rainfall data; and (c) simulating hydrographs. NDVI = normalized difference vegetation index. IMS = Israel meteorology station. WRF-Hydro = Weather Research and Forecasting hydrological model

in terms of LC types was conducted. The available rainfall data for the hydrological year of 2012–2013 were analysed, and then, the hydrological model was calibrated. Next, the model was simulated for two selected rainfall events. The three LC maps were used as input layers for the model run-off simulations with each storm event, and the run-off simulations were analysed.

2.2.1 | LC maps

LC maps were derived through satellite imagery, acquired by the Advanced Spaceborne Thermal Emission and Reflection Radiometer (ASTER) sensor. The choice to use ASTER sensor images was based on the sensor's high spatial resolution (15 m) while using nine visible and near and shortwave infrared spectral bands (Abrams, Hook, & Ramachandran, 2002). ASTER provided an image acquired on December 9, 2010, 3 days after the fire was extinguished, making it the best option available. Two additional images were chosen to represent the prefire and postfire stages from May 20, 2008 to January 15, 2013.

The three images went through atmospheric, topographic, and radiometric corrections using the Atmospheric/Topographic Correction software (Richter, 2010) and followed by a geographic registration. An LC classification was applied, and each image was classified into five different LC types, using a maximum likelihood supervised classification technique (Ozesmi & Bauer, 2002), including built-up areas, forest, agricultural areas, annual vegetation, and bare soils. An accuracy assessment procedure was performed, using the kappa coefficient and an overall accuracy assessment (Foody, 2002). This procedure was conducted using a manual comparison of 500 stratified random points across each map to a 1-m resolution orthophoto of the area. The 2013 image posed a challenge. It was acquired 2 years after the fire event and showed a large area covered with vegetation. Because a 15-m resolution is too coarse to distinguish between forest and annual vegetation, a mosaic of RapidEye images, with a spatial resolution of 5 m, acquired on October 15 and 17, 2013, was created. The normalized difference vegetation index (NDVI) was derived from the red and near-infrared reflectance ratio (Pettorelli et al., 2005) to monitor the state of vegetative areas. The NDVI was applied to the RapidEye mosaic and used a threshold of 0.42, based on other studies, to distinguish between annual vegetation ($0.42 < NDVI < 0.55$) and forest ($NDVI > 0.55$; Baldeck et al., 2014; Faroux et al., 2013; Leeuwen et al., 2010). The area with an NDVI between 0.42 and 0.55 was considered to be covered by annual vegetation and was integrated into the ASTER 2013 classified map. Finally, a basic analysis of LCC was conducted by summing the number of pixels representing each of the five classes for every image and comparing the three images to analyse the LCCs.

2.2.2 | Cover types sensitive to fire

Survey of Israel and Israel Nature and Parks Authority maps were used to assess the sensitivity of different vegetation categories to fire. First, the burnt area was calculated by dividing the 2008 classification map by the 2010 map to detect the pixels that underwent a change from forest to the bare soil. Only the pixels that were located within the fire area defined by Tessler et al. (2011) were considered as burnt area. Next, the Survey of Israel land-use map was used to calculate the percentage of areal cover of each LC type within the Oren sub-basin. The same calculations were conducted only within the burnt area. This way, the relative areal cover of the different LC types in the whole sub-basin with the relative portion that these LC types occupied in the burnt area could be compared. For the two most common vegetated LC types (planted and natural forest), the density of the vegetation (high, medium, low, and sparse) was analysed, using the Israel Nature and Parks Authority's map of measured vegetation cover via remote sensing. The areal cover percentage of the density categories of planted and natural forest across the entire sub-basin area was also compared.

2.2.3 | Rainfall events

The record shows that the winter season of 2012–2013, 2 years after this fire, was characterized by both severe drought conditions prior to the wet season and extreme flood events due to above normal precipitation. This was true in terms of the number of rain days, the rain intensity, and the total rainfall amounts during several storm events, causing unusually high discharge levels in most of the Carmel Forest's watersheds. The two rainfall events that were chosen for this study occurred on December 20–21, 2012 and January 6–10, 2013. The first has a recurrence time of almost every year; the second rainfall event has a recurrence interval of 2.5% and is considered to be rare due to its duration of 5 days. Examining frequent and extreme rainfall events enabled us to learn about the run-off response to fire in both scenarios.

2.3 | Uncoupled WRF-Hydro hydrological model

The uncoupled version of the WRF-Hydro model was recently adopted and calibrated by the Israel Water Authority (Givati et al., 2016). It is a stand-alone one-way version of the original WRF-Hydro model designed by the National Center for Atmospheric Research. The WRF-Hydro extension package provides a framework for simulating surface run-off, groundwater flow, and channel routing (Silver, Karnieli, Ginat, Meiri, & Fredj, 2017). It allows for a multiscale representation of terrestrial hydrological processes linked to the spatial redistribution of surface, shallow subsurface, and channel water across the terrain (Givati et al., 2016). The model provides multiple physics options for surface overland flow, saturated subsurface flow, channel routing, and baseflow dynamics. It relies on the Noah land surface model for data such as topography, land cover, soil types with their relevant soil moisture content, infiltration capacity excess, and hydraulic conductivity (Yucel, Onen, Yilmaz, & Gochis, 2015). It is a flow model that is aimed at simulating hydrographs for specific rainfall events. Terrain routing and, subsequently, channel and reservoir routing functions can be implemented into the one-dimensional Noah land surface model (Mitchell, 2005). Its design was motivated by the need to account for increased complexity in land surface states and fluxes and to provide stream channel discharge information for hydrometeorological applications. The uncoupled WRF-Hydro model that was used in this study integrates the WRF meteorological model forecasting technique or measured rainfall data from meteorological stations, forcing these meteorological data into the hydro equations. Additional spatial analyses were carried out using geographic information system software (http://www.esri.com/products, 2016). The uncoupled

WRF-Hydro model was designed to calculate both specific run-off values at locations along the watershed and a watershed hydrograph.

2.3.1 | The model structure and inputs

In this current study, the uncoupled WRF-Hydro model based the calculations on interpolation of the measured rainfall data. The following input files are required: (a) a layer of the watershed(s) domain; (b) a soil-type raster map and an LC raster map, along with tabulated empirically based run-off coefficients for each soil type and LC type; (c) Manning roughness coefficients and a hydraulic radius table, calculated for each watershed; (d) slope, flow direction, and flow accumulation maps derived from a digital elevation model (DEM); and (e) rain and soil moisture, based on a calculation of soil moisture from accumulated rainfall and slope values. Two major steps must be performed and are specified in detail in Appendix A. The first step includes run-off calculation. The rainfall data, the run-off coefficient table, the soil map, the LC map, and the DEM products are used to derive a run-off point feature class and an accumulated rainfall point grid. During this step, the outputs include a rainfall layer, in which each point is assigned rainfall and soil moisture values for each time step, as well as slope, LC, and soil-type values; the second product is a run-off grid, in which discharge values (m^3/s) are assigned to every point in the grid for each time step. The second step consists of hydrograph calculations. This step accounts for the accumulated rainfall point grid, the Manning roughness coefficients and the hydraulic radius table, and the DEM-derived files. The output is a velocity raster (see Appendix A for further details). The velocity raster is then used to calculate the concentration time to the outlet of the watershed. Together with the run-off point feature class, the watershed hydrograph is calculated.

2.3.2 | Uncoupled WRF-Hydro calibration and simulation

The main parameters for calibrating the model include those for setting the amount of surface water for a given volume of precipitation and for determining the water movement from the slopes and channels and consequently the hydrograph shape. The model allows a Manning roughness coefficient to be set for each stream order in the domain. The model's channel routing parameters are defined as functions of stream order values. The routing parameters determine how fast water moves across the terrain and into stream and river channels. The rougher the surface, the longer it takes for water to reach the channels, and slow water movement enables higher infiltration rates into the soil. Eventually, the roughness parameter affects both the timing and the amount of streamflow simulated by the model. Larger stream orders towards the watershed outlet are characterized by lower Manning roughness coefficients and increased water velocity and discharge in the channels. The model contains a runoff coefficient table for overland flow as a function of various soils and land-cover types.

Calibration of the model was conducted by comparing four simulated storm events between 2012 and 2015 to measured run-off discharge and volume values. The percent difference between the parameters (run-off volume and peak discharge) of the in situ measured run-off against the simulated run-off was calculated. If there was a large bias between the model results and the in situ measurements, a calibration procedure was performed by adjusting the run-off coefficients. Normalized root mean square errors (NRMSE) were also considered for simulation performance evaluation (Ranatunga, Tong, & Yang, 2017). The Oren Hydrometric Station has been operational only since 2012; therefore, there was limited data available for calibration. The January 2013 classification map was used for model calibration to represent the LC status at the time of the rainfall events used for calibration, and the measured rainfall data sets were used for the calibration procedure. Because LCCs during this time period (after the fire event and on) were rapid, and the landscape changed frequently, the calibration using the 2013 LC map could only be conducted with hydrological events that occurred 2 years before or after 2013, so that the LC spatial patterns were accounted for. The Oren Stream does not generate medium–large flows very often, so for the time period that was determined for calibration considering the 2013 LC map, there were six rainfall events to rely on for calibration and validation. The uncoupled WRF-Hydro model was operated with two rainfall events from the hydrological year of 2012–2013 (December 20–21, 2012 and January 6–10, 2013). Three different simulations were conducted for each rainfall event, each time using one of the three LC maps. This was performed to understand how a certain rainfall event, together with the three different LC stages of the watershed (prefire, postfire, and regeneration), would affect the run-off response. The hydrograph, peak discharge, and run-off volume results were then compared.

3 | RESULTS

3.1 | LC maps

The three LC maps that were derived from the ASTER satellite images are presented in Figure 3. The largest changes between 2008 (Figure 3 a) and 2010 (Figure 3b) were a 24.1% increase in the rock and bare soil class and a reduction of 25% in the forest LC. A slight increase in forest areas (~5.8%) occurred between 2010 (Figure 3b) and 2013 (Figure 3 c). Moreover, in 2013, ~17% of the study area was covered by annual vegetation. There was also a slight increase in the portion of urban area out of the total area. In 2013, there was a larger portion of the area covered by agricultural landscape, which was clustered in a specific location (Figure 3c). This is due to the difference in seasonality between the 2008 (acquired in May) image and the 2013 image (acquired in January). Because no other satisfying data set was available from ASTER during wintertime between the years 2007 and 2009, this image was chosen, as it clearly represents the status of the evergreen forest 2.5 years before the fire event. The accuracy assessment results of the classification maps were satisfactory, with ~88–93% overall classification accuracy (Table 1).

3.2 | Burnt area analysis

The Oren sub-basin covers an area of 24.17 km^2, characterized mainly by planted forest, mostly pines (43%; Figure 4). The LC type named "no characteristic" is mostly composed of built-up area and occupies 17% of the sub-basin area, as do the shrubs. Natural forest covers 9% of the area, and the remaining LC types cover <6% (cultivated area, fallow land, stony area, and orchards). The fire consumed an area mostly covered by continuous areas of planted forest, with patches of natural

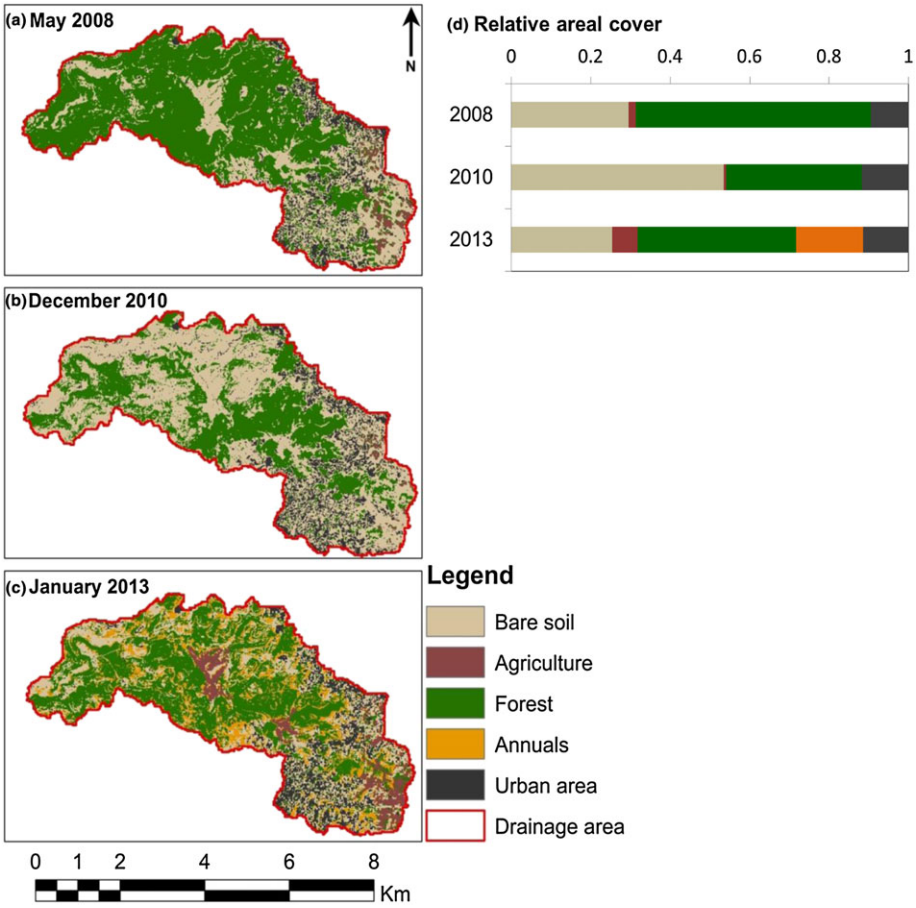

FIGURE 3 The land-cover maps for the three time periods that were studied: (a) May 2008, (b) December 2010, and (c) January 2013. Panel (d) qualitatively shows the relative areal cover of each land-cover type in each year

TABLE 1 Accuracy assessment results for the three land-cover maps

Land-cover map	Overall classification accuracy (%)	Kappa statistic
2008	40.88	83.0
2010	58.89	84.0
2013	20.93	91.0

forest, shrubs, and cultivated land. The burnt area covered 5.93 km^2, which is 24.5% of the total sub-basin. We calculated the areal cover of the LC types that used to consume the area affected by the fire, in order to determine the most sensitive LC cover types. The area affected by the fire was also composed mostly of planted forest; this LC type covered 80% of the burnt area before the fire. Shrubs occupied 10% of the burnt area before the fire, and natural forest used to

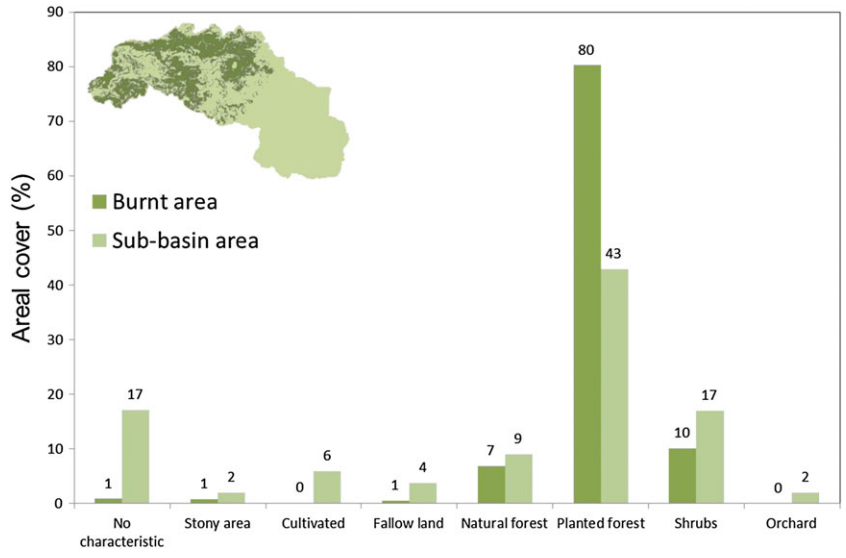

FIGURE 4 Percent areal cover of different land-cover types. Light green bars represent the relative cover of the entire Oren sub-basin, whereas dark green bars express the portion cover of the burnt area within the sub-basin. The illustration on the upper-left part of the figure shows the burnt area locations within the Oren sub-basin

cover 6.9%. The other LC types each compose <1% of the burnt area. Before the fire occurred, planted forest covered 43% of the total sub-basin but showed a very high sensitivity to fire with 80% of the burnt area previously composed of planted forest. The "no characteristic" LC (mostly urban area) covered 17% of the sub-basin but showed a high resistance to the fire event, constituting <1% of the burnt area. The natural forest category showed lower flammability with 7% of this LC type previously covering the burnt area, compared to 9% that covered the entire sub-basin area. The same goes for shrubs (10% of burnt area vs. 17% of entire sub-basin).

Medium density forest was the most sensitive to fire, in both natural and planted forest, and occupied 56.85% and 47.44% of the total burnt area, respectively; this is compared to 43.4% coverage of medium density forest and shrubs in the entire sub-basin area. Medium-high density planted forest was much more sensitive to fire than medium-high density natural forest, covering 42.07% (which is above the cover percentage value of the entire sub-basin: 34.71%) and 16.24% of the total burnt area (about half the cover percentage of the sub-basin), respectively. In low-medium density forest, natural forest was more sensitive to fire, with 17.29% of the burnt area for this category (and above the cover percentage value of the entire sub-basin: 12.97%), compared to only 7.04% of low-medium density planted forest burnt (below the sub-basin's cover percentage). Comparison between the postfire and regeneration stages showed a large increase in vegetation cover, mostly annuals (+17%) and forest cover (+5.79%), and agricultural activity (+5.65%) attributed to the season in which the satellite image was acquired.

3.3 | Hydrological modelling

The Oren Stream Hydrometric Station has been operational only since 2012; therefore, relatively few hydrological events were available for calibration. Moreover, rainfall events with different rainfall (and run-off) magnitudes behave differently in terms of run-off coefficients and soil moisture, so a rough generalization was needed to comply with all types of hydrological responses. Two run-off events were used for validation. For maximum discharge and run-off volume, the average errors were 34% and 22.5%, respectively. NRMSE varied between 0.77 and 1.44 m^3/s, with more accurate hydrological simulations for larger rainfall events than for smaller ones (Table 2).

Two rainfall events from the hydrological year of 2012–2013 were chosen to simulate hydrographs that represent the effects of wildfire on the rainfall–run-off relationship (Figure 5). They were simulated three times using the uncoupled WRF-Hydro model, and each simulation used a different LC map (Figure 3a–c). The measures of both peak discharge and run-off volume showed a large increase between the results of the simulation using the 2008 LC image and the 2010 image (between 39% and 47%). For the 2013 image simulations, the results showed a decrease in both peak discharge and run-off volume values (between 7.7% and 9%). The large increase in the 2010 LC image is a direct result of the wildfire event of December 2010 and the transition of large portions of the watershed from forested to exposed rock and bare soil (Figure 3). There was a moderate decrease in the discharge and run-off volume (Figure 5) for the 2013 LC image simulation. In terms of run-off magnitude, both run-off events responded quite similarly to the wildfire event. The December 20–21, 2012 event (recurrence time of almost 1 year) showed larger increases in both maximum discharge and run-off volume values after the fire took place than did the extreme event of January 6–10, 2013. There was also a greater decrease in these values 2 years after the fire event (Figure 5).

4 | DISCUSSION

The effects of forest composition and species distribution on wildfire were studied, as well as the impact of fire on LCC and rainfall–run-off relations during large rainfall events. The results show that during the postfire stage, about 24% of forest cover was lost due to the December 2010 fire in Mount Carmel, Israel. The main forest loss occurred in areas covered by planted forest, specifically pines, which composed 80% of the burnt area. More than half of the burnt area was composed of medium density forest, making it the most sensitive to fire. In addition, we studied the effect of wildfire on the run-off regime and found that during the postfire stage, maximum discharge and run-off volume values increased by 39–47% compared to prefire. These results imply that prefire management practices had a significant impact on postfire hydrological processes. As the annuals and forest regenerated, the peak discharge decreased by up to 9%. Hydrological responses to larger postfire rainfall events that last several days (in this study, 5 days) generate fewer differences compared to prefire, possibly because the variability of soil moisture is lower during most of the hydrological event. Common events are more likely to have a greater response to LCC due to fire.

In addition to causing LCC, wildfires are greatly affected by LC spatial patterns and are usually the result of human disturbance and climate conditions (Paz et al., 2011; Wittenberg & Inbar, 2009). Their effects on the watershed landscape are mostly immediate (Moody & Martin, 2001). Uncontrolled wildfires may consume large areas,

TABLE 2 Rainfall events used for calibration and validation, along with their run-off volume and maximum discharge values, as measured by the hydrometric station and NRMSE

	Rainfall events by dates	Maximum discharge (m^3/s)	Run-off volume (10,000 m^3)	Maximum discharge percent difference	Run-off volume percent difference	NRMSE
Calibration	December 20–21, 2012	12.28	29.26	−42.09	−43.77	0.78
	January 6–10, 2013	10.05	53.82	−29.78	−19.93	1.01
	January 30–31, 2013	2.5	7.49	58.13	31.22	1.26
	January 10–11, 2015	4.13	4.11	3	76.6	1.03
Validation	December 12–14, 2013	1.7	7.97	−15.02	16.24	1.25
	January 19–20, 2016	0.65	0.75	−52.94	−28.77	1.44

Note. NRSME = normalized root mean square error.

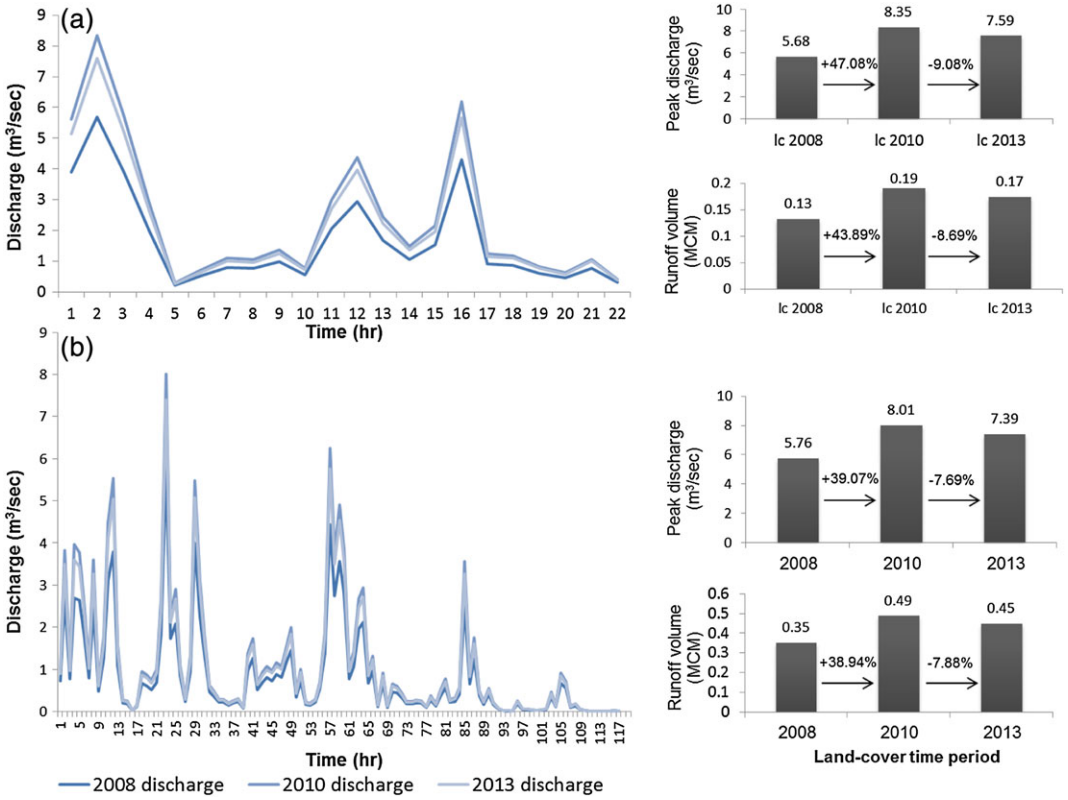

FIGURE 5 Simulated hydrographs for the two rainfall events: (a) December 20–21, 2012 and (b) January 6–10, 2013. The bar graphs on the right show the changes in peak discharge and run-off volume between the studied time periods. lc = land-cover

causing dramatic alterations in LC within hours/days. In the current study, the LC maps demonstrate that about 24% of the research area shifted from a forested landscape to bare soil due to the fire. Between 2008 and 2010, the peak discharge increased by 39–47% and the run-off volume by 39–44%. Forest fires continue to be a recurring phenomenon in the Mediterranean basin and specifically in Israel. The return interval of large fires (500 ha) in Mount Carmel is 17 years. Small fires (5–10 ha) occur every year with a probability of 87% (Tessler, 2012). The December 2010 fire covered >2,500 ha in Mount Carmel and caused the loss of 38% of the Oren Watershed's forest cover (Tessler et al., 2011). These trends are expected to accelerate and have a consequent effect on forest fires in terms of burnt areas and frequency of events. Soulis et al. (2012) found that a watershed in which 90% of its area was burned experienced an increase of about 850% in maximum peak flow in a postfire rainfall event. In a study conducted in one of the Carmel Forest streams, located near the Oren Watershed, Wittenberg and Inbar, (2009) reported an increase of two orders of magnitude in run-off yields in the first year after a fire (1989), followed by winters in which decreasing amounts of run-off were measured. A study in California (Kinoshita & Hogue, 2015) demonstrated a sharp increase in postfire discharge, and low flow seasons showed an elevated run-off ratio for up to 10 years following the fire.

On Mount Carmel, extensive afforestation processes and changes in the landscape and forest composition during the past 100 years have led to a large amount of planted trees within the forest, 50% of which are *P. halepensis*. This species is presumed to have been rare in the native communities in the past (Volcani, Karnieli, & Svoray, 2005; Wittenberg & Malkinson, 2009). A study by Bosch and Hewlett (1982) found that a reduction in coniferous cover was correlated to a streamflow increase of about 40 mm in annual water yield per 10% change in forest cover, making it the vegetation cover type causing the greatest increase with its removal. Specifically on Mount Carmel, it was reported that the planted *Pinus* forest was more susceptible to fire, and fire severity was higher there (Tessler et al., 2011). These data support the findings of higher sensitivity to fire in planted forest with *P. halepensis*. Natural forest and shrubs were found to be more resistant to fire. The Oren sub-basin was covered by a large area of planted forest before the December 2010 fire, turning these areas into a fire-sensitive environment. In addition, the results suggest that a medium density forest is the most sensitive to fire. A medium-high density planted forest is far more flammable than a medium-high density natural forest. However, in a low-medium density forest, the natural forest was more sensitive to fire than the planted forest. The loss of vegetation cover (planted and native) significantly altered the watershed conditions and run-off response (Githui, Mutua, & Bauwens, 2010; White & Greer, 2006). The findings have important implications for forest management and fire control in the Mediterranean region, specifically regarding decision-making processes related to the types of trees that are being planted in light of afforestation policies and objectives.

The study results show that the burnt area was composed mostly of planted forest, primarily comprising *P. halepensis*, which is a fire-sensitive species, although its seeds are resistant to fire. In broad-leaf species, such as oaks and pistachio, the seeds are sensitive, but the burnt trees easily regenerate from subsurface buds (Keesstra et al., 2017). These differences in species traits will affect the forest recovery after

fire, as well as the forest structure and composition. In general, Mediterranean vegetation is fire-adapted and is therefore highly resilient. However, studies have shown that the relatively high fire frequency on Mount Carmel has gradually shaped the landscape towards homogeneity in which shrubs are the dominant vegetation form (Tessler, Wittenberg, & Greenbaum, 2016). Understanding such mechanisms that affect LCC is essential for better predicting future fire regime and vegetation patterns in fire-sensitive areas, in order to adopt efficient practices and means to mitigate future wildfire consequences in similar Mediterranean regions.

The uncoupled WRF-Hydro model can be used for operative ad hoc forecasting and simulation, providing valuable information for watershed management purposes. It is, therefore, a useful tool for decision-making processes in relevant time scales, as well as for research purposes, such as those discussed in this paper. The calibration process was conducted with a small amount of rainfall events, because the hydrometric station has been operational only since 2012. This is a major limitation in the study, and the model simulations could have reached higher accuracy with a larger data set for calibration. Smaller and shorter rainfall events resulted in higher NRMSE scores that express lower accuracy than for larger events.

Wittenberg and Malkinson (2009) proposed that the fire regime in the Carmel region is a result of increasing human activities, including afforestation and the introduction of non-native trees to the area. Increased numbers of the more flammable pine trees set the stage for large-scale fires. Large fire events may alter the hydrological regime of the watershed within days and have a long-term effect on the run-off regime in the watershed. In the case of the Oren Watershed, the areas downstream are not densely populated and are mostly agricultural. However, under similar events in more urbanized watersheds, fire risk assessments should be considered during the planning process, and afforestation methods, such as species type and forest density, should be selected with an eye towards preventing severe impacts on settlements and their well-being (Paz et al., 2011). Major forest fires in Mediterranean environments occur periodically, with complex effects on hydrological, geomorphological, and ecological processes, due to the complexity of the landscape structure and to different responses of such systems to various LC types. Expected trends of longer drought periods will increase the risk of fire, and the ongoing trend of more extreme rainfall events creates the need to simulate and evaluate the effects of LCC on the hydrological regime. Integrated approaches that include forest composition, species distribution, and hydrological processes in the landscape scale can improve management and fire control in this Mediterranean region.

5 | SUMMARY AND CONCLUSIONS

The current study demonstrates the differences in the fire sensitivity of planted and natural forest trees and the effects that one severe fire had on the run-off response on a watershed scale. An unusual season of rainfall events during 2012–2013 provided the opportunity to study the impacts of both a dramatic LCC caused by wildfire and a rare rainfall event on the hydrological processes. It was found that LC has changed dramatically due to the wildfire, leaving about 24% of the areas that were covered by forest, bare and exposed. A planted forest composed of pines is highly sensitive to fire, especially when its density is medium or medium-high. The LCCs led to a large alteration in the run-off response, with a peak discharge increase of ~39–47% and a run-off volume increase of ~39–44%. The vulnerability of this area, along with increasing periods of dry spells and droughts in the Mediterranean region, suggests that there is an expected increase in future wildfires that may cause effects similar to the ones found in this study. The results show that the first 2 years of regeneration resulted in a decrease in maximum discharge (7.7–9%) and run-off volume (7.9–8.7%). As the forest goes through its succession process of postfire recovery, it is expected that the rainfall–run-off response will continue to decrease, unless recurring fire events introduce additional disturbances to the ecosystem. High intensity rainfall events, following the large impact of fire, may endanger both the well-being of the population and the infrastructure, as well as create an additional disturbance to the ecosystem in the form of high sediment yields and nutrient loss.

ACKNOWLEDGEMENTS

This research was partly supported by the Israel Water Authority (study number 4500686906); by the Ministry of Science and Technology via the Ramon Foundation, Israel (contract 3-10673); and by the European Union's Horizon 2020 Research and Innovation Programme under grant agreements 641762 (Ecopotential) and 654359 (eLTER). We also would like to acknowledge the Jewish National Fund for their support and contribution to this study. A special thanks to Natalya Panov for her assistance and advice and to Dror Paz for his professional support regarding the WRF-Hydro model.

ORCID

Noa Ohana-Levi http://orcid.org/0000-0002-6909-7934
Arnon Karnieli http://orcid.org/0000-0001-8065-9793

REFERENCES

Abrams, M., Hook, S., & Ramachandran, B. (2002). ASTER user handbook, version 2: Advanced spaceborne thermal emission and reflection radiometer. Jet Propulsion Laboratory/California Institute of Technology.

Baldeck, C. A., Colgan, M. S., Feret, J. B., Levick, S. R., Martin, R. E., & Asner, G. P. (2014). Landscape-scale variation in plant community composition of an African savanna from airborne species. *Ecological Applications*, *24*(1), 84–93.

Bosch, J. M., & Hewlett, J. D. (1982). A review of catchment experiments to determine the effect of vegetation changes on water yield and evapotranspiration. *Journal of Hydrology*, *55*, 3–23.

Costa, M. H., Botta, A., & Cardille, J. A. (2003). Effects of large-scale changes in land cover on the discharge of the Tocantins River, Southeastern Amazonia. *Journal of Hydrology*, *283*(1–4), 206–217. https://doi.org/10.1016/S0022-1694(03)00267-1.

Cydzik, K., & Hogue, T. (2009). Modeling postfire response and recovery using the hydrologic engineering center hydrologic modeling system (HEC-HMS). *Journal of the American Water Resources Association*, *45*(3), 702–714. https://doi.org/10.1111/j.1752-1688.2009.00317.x.

Faroux, S., Tchuente, A. T. K., Roujean, J. L., Masson, V., Martin, E., & Moigne, P. L. (2013). ECOCLIMAP-II/Europe: A twofold database of ecosystems and surface parameters at 1 km resolution based on satellite information for use in land surface, meteorological and climate

models. *Geoscience Model Development*, *6*, 563–582. https://doi.org/10.5194/gmd-6-563-2013.

Foody, G. M. (2002). Status of land cover classification accuracy assessment. *Remote Sensing of Environment*, *80*(1), 185–201. https://doi.org/10.1016/S0034-4257(01)00295-4.

Fox, D. M., Laaroussi, Y., Malkinson, D., Maselli, F., Andrieu, J., Bottai, L., & Wittenberg, L. (2016). POSTFIRE: A model to map forest fire burn scars and estimate runoff and soil erosion. *Remote Sensing Applicaitons: Society and Environment*, *4*, 83–91.

Frankenberg, E., & Cohen, Y. (1996). The Carmel project: Declaring of the Carmel as a biosphere reserve. *Ecology and Environment*, *3*, 121–126 (in Hebrew).

Githui, F., Mutua, F., & Bauwens, W. (2010). Estimating the impacts of land-cover change on runoff using the soil and water assessment tool (SWAT): Case study of Nzoia catchment, Kenya. *Hydrological Sciences Journal*, *54*(5), 899–908. https://doi.org/10.1623/hysj.54.5.899.

Givati, A., Gochis, D. J., Rummler, T., & Kunstmann, H. (2016). Comparing one-way and two-way coupled hydrometeorological forecasting systems for flood forecasting in the Mediterranean region. *Hydrology*, *3*(19). https://doi.org/10.3390/hydrology3020019.

Goodrich, D. C., Canfield, H. E., Burns, S., Semmens, D. J., Miller, S. N., Hernandez, M., … Kepner, W. G. Rapid post-fire hydrologic watershed assessment using the AGWA GIS-based hydrologic modeling tool. In American Society of Civil Engineers Watershed Management Conference, Williamsburg, VA, USA, July 19–22, 2005 2005: American Society of Civil Engineers (ASCE)

Green, J. I., & Nelson, E. J. (2002). Calculation of time of concentration for hydrologic design and analysis using geographic information system vector objects. *Journal of Hydroinformatics*, *4*(2), 75–81.

Haim, A., & Izhaki, I. (1994). Changes in rodent community during recovery from fire: Relevance to conservation. *Biodiversity and Conservation*, *3*, 573–585.

Hallema, D. W., Sun, G., Caldwell, P. V., Norman, S. P., Cohen, E. C., Liu, Y., … McNulty, S. G. (2016). Assessment of wildland fire impacts on watershed annual water yield: Analytical framework and case studies in the United States. *Ecohydrology*, *10*. https://doi.org/10.1002/eco.1794.

http://www.esri.com/products (2016).

Inbar, M., Tamir, M., & Wittenberg, L. (1998). Runoff and erosion processes after a forest fire in Mount Carmel, a Mediterranean area. *Geomorphology*, *24*(1), 17–33. https://doi.org/10.1016/S0169-555X(97)00098-6.

Johansen, M. P., Hakonson, T. E., & Breshears, D. D. (2001). Post-fire runoff and erosion from rainfall simulation: Contrasting forests with shrublands and grasslands. *Hydrological Processes*, *15*(15), 2953–2965. https://doi.org/10.1002/hyp.384.

Jolly, W. M., Cochrane, M. A., Freeborn, P. H., Holden, Z. A., Brown, T. J., Williamson, G. J., & Bowman, D. M. J. S. (2015). Climate-induced variations in global wildfire danger from 1979 to 2013. *Nature Communications*, *6*, 7537 (2015), doi:https://doi.org/10.1038/ncomms8537.

Keesstra, S., Wittenberg, L., Maroulis, j., Sambalino, F., Malkinson, D., Cerda, A., & Pereira, P. (2017). The influence of fire history, plant species and post-fire management on soil water repellency in a Mediterranean catchment: The Mount Carmel range, Israel. *Catena*, *149*, 857–866. https://doi.org/10.1016/j.catena.2016.04.006.

Kinoshita, A. M., & Hogue, T. (2015). Increased dry season water yield in burned watersheds in Southern California. *Environmental Research Letters*, *10*, 014003. https://doi.org/10.1088/1748-9326/10/1/014003.

Lane, P. N. J., Sheridan, G. J., & Noske, P. J. (2006). Changes in sediment loads and discharge from small mountain catchments following wildfire in south eastern Australia. *Journal of Hydrology*, *331*, 495–510.

Leeuwen, W. J. D. v., Casady, G. M., Neary, D. G., Bautista, S., Alloza, J. A., Carmel, Y., … Orr, B. J. (2010). Monitoring post-wildfire vegetation response with remotely sensed time-series data in Spain, USA and Israel. *International Journal of Wildland Fire*, *19*, 75–93.

Levin, N., & Heimowitz, A. (2012). Mapping spatial and temporal patterns of Mediterranean wildfires from MODIS. *Remote Sensing of Environment*, *126*, 12–26.

Mitchell, K. (2005). *The community Noah land-surface model (LSM): User's guide public release version 2.7.1*. Washington, D.C.: National Center for Environmental Prediction.

Moody, J. A., & Martin, D. A. (2001). Post-fire, rainfall intensity-peak discharge relations for three mountainous watersheds in the western USA. *Hydrological Processes*, *15*, 2981–2993. https://doi.org/10.1002/hyp.386.

Ne'eman, G., Lahav, H., & Izhaki, I. (1995). Recovery of vegetation in a natural east Mediterranean pine forest on Mount Carmel, Israel as affected by management strategies. *Forest Ecology and Management*, *75*, 17–26.

Osem, Y., Ginsberg, P., Tauber, I., Atzmon, N., & Perevolotsky, A. (2008). Sustainable management of Mediterranean planted coniferous forests: An Israeli definition. *International Forestry*, *106*(1), 38–46.

Ozesmi, S. L., & Bauer, M. E. (2002). Satellite remote sensing of wetlands. *Wetlands Ecology and Management*, *10*, 381–402. https://doi.org/10.1023/A:1020908432489.

Papathanasiou, C., Alonistioti, D., Kasella, A., Makropoulos, C., & Mimikou, M. (2012). The impact of forest fires on the vulnerability of peri-urban catchments to flood events (the case of the Eastern Attica region). *Global Nest*, *14*(3), 294–302.

Paz, S., Carmel, Y., Jahashan, F., & Shoshany, M. (2011). Post-fire analysis of pre-fire mapping of fire-risk: A recent case study from Mt. Carmel (Israel). *Forest Ecology and Management*, *262*, 1184–1188. https://doi.org/10.1016/j.foreco.2011.06.011.

Pettorelli, N., Vik, J. O., Mysterud, A., Gaillard, J.-M., Tucker, J., & Stenseth, N. C. (2005). Using the satellite-derived NDVI to assess ecological responses to environmental change. *Trends in Ecology & Evolution*, *20*(9), 503–510. https://doi.org/10.1016/j.tree.2005.05.011.

Ranatunga, T., Tong, S. T. Y., & Yang, Y. J. (2017). An approach to measure parameter sensitivity in watershed hydrological modelling. *Hydrological Sciences Journal 62*(1) 76–92.

Richter, R. (2010). *Atmospheric/topographic correction for satellite imagery, ATCOR-2/3 user guide, version 1.7*. Wessling, Germany: DLR-German Aerospace Center, remote sensing data center.

Rulli, M. C., & Rosso, R. (2007). Hydrologic response of upland catchments to wildfires. *Advances in Water Resources*, *30*, 2072–2086. https://doi.org/10.1016/j.advwatres.2006.10.012.

Silver, M., Karnieli, A., Ginat, H., Meiri, E., & Fredj, E. (2017). An innovative method for determining hydrological calibration parameters for the WRF-Hydro model in arid regions. *Environmental Modelling & Software*, *91*, 47–69.

Soulis, K. X., Dercas, N., & Valiantzas, J. D. (2012). Wildfires impact on hydrological response—The case of Lykorrema experimental watershed. *Global NEST Journal*, *14*(3), 303–310.

Tague, C., Seaby, L., & Hope, A. (2009). Modeling the eco-hydrological response of a Mediterranean type ecosystem to the combined impacts of projected climate change and altered fire frequencies. *Climate Change*, *93*, 137–155.

Tessler, N. (2012). Documentation and analysis of wildfire regimes on Mount Carmel and the Jerusalem hills. *Themes in Israeli Geography (Special Issue of Horizons in Geography)*, *79-80*, 184–193.

Tessler, N., Elbaz, N., Kaplan, D., Shkedy, Y., Rosenberg, B., Cohen, E., … Greenbaum, N. (2011). Post fire management program after the December 2010 fire Mt. Carmel Forest, Israel.

Tessler, N., Wittenberg, L., & Greenbaum, N. (2016). Vegetation cover and species richness after recurrent forest fires in the Eastern Mediterranean ecosystem of Mount Carmel, Israel. *Science of the Total Environment*, In press, doi:https://doi.org/10.1016/j.scitotenv.2016.02.113.

Tessler, N., Wittenberg, L., Malkinson, D., & Greenbaum, N. (2008). Fire effects and short-term changes in soil water repellency—Mt. Carmel,

Israel. *Catena*, *74*, 185–191. https://doi.org/10.1016/j.catena.2008.03.002.

Volcani, A., Karnieli, A., & Svoray, T. (2005). The use of remote sensing and GIS for spatio-temporal analysis of the physiological state of a semi-arid forest with respect to drought years. *Forest Ecology and Management*, *215*(1), 239–250. https://doi.org/10.1016/j.foreco.2005.05.063.

White, M. D., & Greer, K. A. (2006). The effects of watershed urbanization on the stream hydrology and riparian vegetation of Los Penasquitos Creek, California. *Landscape and Urban Planning*, *74*(2), 125–138. https://doi.org/10.1016/j.landurbplan.2004.11.015.

Wine, M. L., & Cadol, D. (2016). Hydrologic effects of large southwestern USA wildfires significantly increase regional water supply: Fact or fiction? *Environmental Research Letters*, *11*(8), 085006.

Wittenberg, L., & Inbar, M. (2009). The role of fire disturbance on runoff and erosion processes—A long-term approach, Mt. Carmel case study, Israel. *Geographical Research*, *41*(1), 46–56. https://doi.org/10.1111/j.1745-5871.2008.00554.x.

Wittenberg, L., Kutiel, H., Greenbaum, N., & Inbar, M. (2007). Short-term changes in the magnitude, frequency and temporal distribution of floods in the Eastern Mediterranean region during the last 45 years—Nahal Oren, Mt. Carmel, Israel. *Geomorphology*, *84*, 181–191. https://doi.org/10.1016/j.geomorph.2006.01.046.

Wittenberg, L., & Malkinson, D. (2009). Spatio-temporal perspectives of forest fires regimes in a maturing Mediterranean mixed pine landscape. *European Journal of Forest Research*, *128*(297), 297–304. https://doi.org/10.1007/s10342-009-0265-7.

Woodsmith, R. D., Vache, K. B., McDonnell, J. J., & Helvey, J. D. (2004). Entiat experimental forest: Catchment-scale runoff data before and after a 1970 wildfire. *Water Resources Research*, *40*(11). https://doi.org/10.1029/2004WR003296.

Yucel, I., Onen, A., Yilmaz, K. K., & Gochis, D. J. (2015). Calibration and evaluation of a flood forecasting system: Utility of numerical weather prediction model, data assimilation and satellite-based rainfall. *Journal of Hydrology*, *523*, 49–66.

How to cite this article: Ohana-Levi N, Givati A, Paz-Kagan T, Karnieli A. Forest composition effect on wildfire pattern and run-off regime in a Mediterranean watershed. *Ecohydrology*. 2018;e1936. https://doi.org/10.1002/eco.1936

APPENDIX A

UNCOUPLED WEATHER RESEARCH AND FORECASTING HYDRO EQUATIONS

A.1 | Inputs for model simulations (run-off amounts and routing):

- a polygon shapefile of the watershed domain;
- slopes raster (%);
- flow direction raster;
- flow accumulation raster;
- soil-type shapefile;
- land-cover shapefile;
- a table of run-off coefficients for specific soils and land-cover types;
- a table of Manning coefficients and hydraulic radius for different parts of the watershed.

A.2 | Run-off calculations

A.2.1 | Run-off volume calculation—for run-off volume created in time step *i* in location *j*:

$$Flow_{ij} = (R_{ij}{}^{*}C_{ij})0.87{}^{*}A, \quad (1)$$

where

- R_{ij} is the rainfall during time step *i* in location *j* (as provided in the input file);
- C_{ij} is the run-off coefficient in time step *i* in location *j* (calculated);
- *A* is the pixel area in the raster.

A.2.2 | Determining the run-off coefficient:

$$C_{ij} = f\left(\sum_{i=1toi}^{i} R_{ij}, S_j, M_{ij}\right), \quad (2)$$

where

- M_{ij} is soil moisture in time step *i* in location *j* (input file);
- S_j is the soil type in location *j* (input file).

Run-off coefficient is calculated during each time step and is dynamic throughout the storm (Table A1).

A1.3 | Hydrograph calculations

A.3.1 | Flow velocity and concentration time

To calculate the hydrograph, first, the velocity should be calculated (Green & Nelson, 2002). According to the velocity, concentration time (the time it takes for water to flow from a certain location in the watershed to its outlet) is then calculated.

TABLE A1 Example of run-off coefficient table

SG	LU	MCLOW	MCUP	RCLOW	RCMID	RCUP
A	2	0.25	0.3	0.02	0.05	0.1
A	1	0.25	0.3	0.05	0.08	0.12
A	7	0.25	0.3	0.05	0.08	0.12
A	5	0.25	0.3	0.02	0.04	0.07
A	6	0.25	0.3	0.02	0.04	0.07
A	8	0.25	0.3	0.06	0.1	0.2
A	4	0.25	0.3	0.03	0.08	0.11
A	9	0.25	0.3	0.06	0.1	0.2
B	2	0.25	0.3	0.05	0.08	0.12
B	1	0.25	0.3	0.05	0.1	0.15
B	7	0.25	0.3	0.05	0.1	0.15
B	5	0.25	0.3	0.05	0.06	0.07

Note. LU = land-cover type; MCLOW = minimal value of soil moisture; MCUP = maximal value of soil moisture; RCLOW = minimal value of run-off; RCMID = value between maximal and minimal run-off values; RCUP = maximal value of run-off; SG = soil type.

$$V = \frac{R^{0.66} * S^{0.5}}{n}, \quad (3)$$

where

- V is water velocity (m/s);
- R is the hydraulic radium (m);
- S is slope;
- n is Manning coefficient (surface roughness).

Flow velocity is calculated separately for slopes and channels:

$$T = \frac{L}{3,600 * V}, \quad (4)$$

where

- T is concentration time (hr);
- L is the length of flow path (m), extracted from the flow direction input raster.

A.3.2 | Flow velocity calculations for slopes and channels

For slopes, the calculation is based on general and uniform parameters for the area of Israel, and for channel calculations, the parameters are unique for each watershed.

- Flow velocity calculation for slopes:

Manning coefficients and hydraulic radius are divided according to Table A2.

- Flow velocity calculation for channels:

Once run-off reaches the channels, the calculations will be according to Equations 3 and 4, where R and n will change according to slope and rainfall accumulation, as specified in Table A3.

TABLE A2 Roughness coefficients and hydraulic radius for flow in slopes

ML	MP	HRL	HRP
0.15	0.12	0.002	0.005

Note. HRL = hydraulic radius for accumulated rainfall of up to 30 mm; HRP = hydraulic radius for accumulated rainfall of over 30 mm; ML = Manning coefficient for accumulated rainfall of up to 30 mm; MP = Manning coefficient for accumulated rainfall of over 30 mm.

TABLE A3 Calculations of hydraulic radius and manning coefficient according to slope and rainfall accumulation

BasID	M_up	M_down	HRL	HRM	HRP
64	0.045	0.04	0.15	0.7	1.4
2	0.045	0.035	0.1	0.3	0.5
3	0.035	0.055	0.1	0.3	0.5
4	0.045	0.03	0.1	0.6	1
5	0.045	0.035	0.1	0.5	1.2
169	0.045	0.03	0.2	0.7	1.4
8	0.04	0.03	0.1	0.5	1.2
183	0.05	0.035	0.1	0.4	1
11	0.045	0.035	0.1	0.5	0.8

Note. BasID = watershed's ID number; HRL = hydraulic radius (R) for accumulated rainfall of up to 30 mm; HRM = hydraulic radius (R) for accumulated rainfall between 30 and 50 mm; HRP = hydraulic radius (R) for accumulated rainfall of over 50 mm; M_up = Manning coefficient (n) for slopes >2%; M_down = Manning coefficient (n) for slopes <2%.

A.3.3 | Hydrograph calculations

Time calculation: The total time of channel flow will be the sum of time intervals calculated according to Equation 3 in the slopes and channels. For each location in the watershed, a time grid is calculated and states the hours it takes for water to flow to the pour point of the watershed.

Volume calculation: According to the time grid calculations, the area that flows during each hour is known. This area multiplied by the run-off (mm) will provide the hourly volume. The division of the volume by time will provide the discharge (m^3/s) and the accumulated volume (m^3).